Mediterranean Geoscience Reviews (2024) 6:233–248
https://doi.org/10.1007/s42990-024-00137-3

ORIGINAL PAPER

Enhancing geotechnical zoning through near-surface geophysical surveys: a case study from eastern Agadir, Morocco

Ismaail Khadrouf[1] · Ouafa El Hammoumi[1] · Najib El Goumi[2] · Abdessamad El Atillah[3] · Youssef Raddi[4] · Mostafa Oukassou[1]

Received: 30 April 2024 / Revised: 6 August 2024 / Accepted: 7 August 2024 / Published online: 30 August 2024

Abstract

The eastern Agadir (Morocco) was selected for the urban expansion. However, it faces challenges owing to its location within an alluvial basin of weak and heterogeneous sediments, compounded by the scarcity of geotechnical data. This study aimed to create the first geotechnical zoning map of the area to support informed urban planning. Geophysical surveys were employed with available in situ investigations to address this data gap and delineate and characterize the main geotechnical zones. The electrical resistivity tomography (ERT) method was used to map the soil distribution horizontally and vertically, complemented by laboratory tests. The multichannel analysis of surface waves (MASW) and seismic refraction tomography (SRT) methods provided insights into important geotechnical and elastic-dynamic parameters. This analysis revealed three distinct geoseismic layers. The surface layer consisted of sand, silt, pebble, weathered limestone, and marlstone, whereas the underlying layer contained compacted silt, dense sand, conglomerate, sandstone, limestone, and marlstone. This layer exhibited higher seismic velocities and lower soil heterogeneity than the surface layer. The third layer, characterized by limestone, marlstone, and compacted deposits, serves as geotechnical bedrock. The V_{S30} velocities were calculated and classified according to the EUROCODE 8 scheme, which categorizes sites based on their geological characteristics and associated seismic risks. The study area was divided into Class A (rock), Class B (dense soil and soft rock), and Class C (medium dense sand and gravel). This classification is essential for assessing seismic response and designing earthquake-resistant structures. The majority of the sites were categorized as Class B. The final zoning map reveals five distinct geotechnical zones: Tagragra's Dome, the alluvial fans and floodplain, the alluvial terrace, the limestone plateau, and the sand dune zone. The calculated parameters revealed soil heterogeneities in horizontal and vertical directions. These results provide valuable key parameters for informed urban planning, with special attention paid to areas with weak soil during foundation design.

Keywords Eastern Agadir · Near-surface geophysical surveys · Geotechnical zoning map

✉ Ismaail Khadrouf
ismaail.khadrouf-etu@etu.univh2c.ma

[1] Laboratory of Applied Geology, Geoinformatics and Environment, Department of Geology, Faculty of Sciences Ben M'sick, Hassan II University, Casablanca, Morocco

[2] Georesources Laboratory, Earth Sciences Department, Faculty of Science and Technology, University of Cadi Ayyad, BP549, Marrakech, Morocco

[3] Spaces, Societies, Environment, Planning and Development Laboratory, Department of Geography and Planning, Faculty of Languages, Arts and Human Sciences-Ait Melloul, Ibnou Zohr University, Ait Melloul, Morocco

[4] Department "Sciences de La Terre", Faculty of Sciences Agdal, Mohamed V University, BP 1014, Rabat Agdal, Morocco

1 Introduction

Rapid urbanization and population growth experienced by many cities worldwide, including Agadir in Morocco, have necessitated implementing new land-use and civil planning measures to accommodate the increasing demands for modern living, roads, and industrial infrastructure. However, this urban transformation brings a pressing need for comprehensive knowledge about the geological and geotechnical properties of soil and rock to ensure the safety of buildings, the long-term viability of engineering structures, and rational planning and sustainability (Karastathis et al. 2010; Muztaza et al. 2022). Insufficient or inadequate soil characterization can lead to unsatisfactory engineering designs, which may result in severe construction problems or even catastrophic

structural failures. To prevent such hazards, geotechnical zoning maps provide essential information for various purposes, including details on the geotechnical properties of materials, vertical and horizontal soil distributions, bedrock depth, groundwater levels, and environmental assessments (Karastathis et al. 2010; Berhane and Walraevens 2012; El May et al. 2015; Failache and Zuquette 2018; Timoulali et al. 2022). On the other hand, it is worth noting that creating these maps requires a substantial amount of in-situ and laboratory data, incurring high costs and time-consuming efforts, resulting in spatially limited data (Calamita et al. 2023). To address these challenges, various studies have used subsurface geophysical investigations to assess the suitability of near-surface materials. These investigations provide valuable information related to the geological, geotechnical, and seismic conditions of subsurface layers (Pegah and Liu 2016; Mohammed et al. 2020; Hasan et al. 2021; Ishak et al. 2022; Zaid et al. 2022; Bello et al. 2022; Ayele et al. 2022; Khadrouf et al. 2024). In addition, several useful correlations exist between the measured physical parameters and the geotechnical items.

The selection of geophysical methods for geotechnical evaluation is guided by the nature of the target problem and site criterion (target depth, resolution, terrain accessibility, and cost) (Al-Heety et al. 2021). Among these methods, electrical resistivity tomography (ERT), multichannel analysis of surface waves (MASW), and seismic refraction tomography (SRT) have been widely used for accuracy, non-invasiveness, efficiency, and cost-effectiveness for determining the geometry, as well as the geotechnical properties of soil materials. However, geophysical surveys have several limitations, such as penetration depth, and resolution, non-uniqueness of data, and sensitivity to anthropogenic sources (Lin et al. 2015). The preferred approach is to use multiple geophysical surveys alongside available geotechnical investigations to reduce limitations and minimize ambiguities. To achieve this, we integrate geophysical methods with geotechnical measurements.

Several cities in Morocco have expanded without a thorough understanding of the geotechnical and geomorphological soil conditions, contributing to constructive problems and potential natural hazards. Few geotechnical maps have been produced for Morocco, mainly emphasizing well-known urban areas and metropolitan cities. These maps, originating from the 1960s and the 1970s, primarily focus on describing geological and geomorphological surface characteristics, neglecting the geotechnical and elastic-dynamic properties of soils and rocks (e.g., Jeannette 1965; Humbert 1966; Mazéas 1967).

Despite the strategic and economic importance of Agadir City, there is a lack of studies or maps focusing on geotechnical soil characterization. Furthermore, this area is situated within a deep and heterogeneous alluvial basin of fluvial-lacustrine and aeolian sediments, making it vulnerable to liquefaction, site effects, soil erosion, and groundwater contamination (Malki et al. 2016; Elmouden et al. 2016; Bouaakkaz et al. 2023; Khadrouf et al. 2024). Additionally, this area is prone to flood and seismic hazards, such as the 1960 Agadir earthquakes, which destroyed 75% of the city, even with a moderate magnitude (Mw = 5.9), and highlighted the vulnerability of its buildings (Sébrier et al. 2006; El Morjani et al. 2016).

Therefore, this study aimed to use subsurface geophysical surveys as a reliable alternative to traditional geotechnical data to address the scarcity of in situ investigations and laboratory tests in the area. In this regard, the ERT method was employed, supplemented by field studies and available laboratory tests, to delineate the main geotechnical units of the study area. P-waves from the SRT and S-waves from the MASW were used to characterize these units and estimate their geotechnical, petrophysical, seismic, and elastic engineering characteristics. The results were integrated and analyzed to produce a comprehensive geotechnical zoning map.

2 Geological and seismic sitting

The study area is located in the eastern part of Agadir City (Morocco) and lies between latitudes 30.443° N and 30.327° N and longitudes − 9.574° W and − 9.354° W. It was selected as a planned city extension. This area is part of the Souss Basin a faulted syncline delineated to the north by the active High Atlas Mountains and to the south by the Anti-Atlas Mountains (Ambroggi 1963). The basin consists of a Paleozoic schist basement overlain by thick Cretaceous–Eocene strata, and its subsurface is further, characterized by Plio-Quaternary sediments of fluvio-lacustrine and eolian origin. Fluvio-lacustrine sediments include alluvial fans (limestone blocks, sand, silt, and poorly cemented conglomerates), cemented alluvial fans (silt, limestone, and sandstone), and river terrace deposits (silt, clay, and sand). Eolian sediments consist of sand fields and dune accumulations (Aït Hssaine and Bridgland 2009) (Fig. 1). These sediments exhibited heterogeneity in vertical and lateral directions. The seismotectonic context of this region is related to the interaction between the African and Eurasian Plates. This tectonic activity likely started during the Late Cretaceous and continued at an approximate rate of 3- to 5 mm/year in a northwest-to-southeast direction (Dewey et al. 1989; Tahayt et al. 2008). The main structural feature in this area is the South Atlas Front, which has affected the northern edge of the Souss Basin with a WSW−ENE fault network extending roughly 150 km. From west to east, this area is bounded by four segment fault tracts: the 30-km long Agadir–Tagragra Fault oriented WNW-ESE, the 35-km long

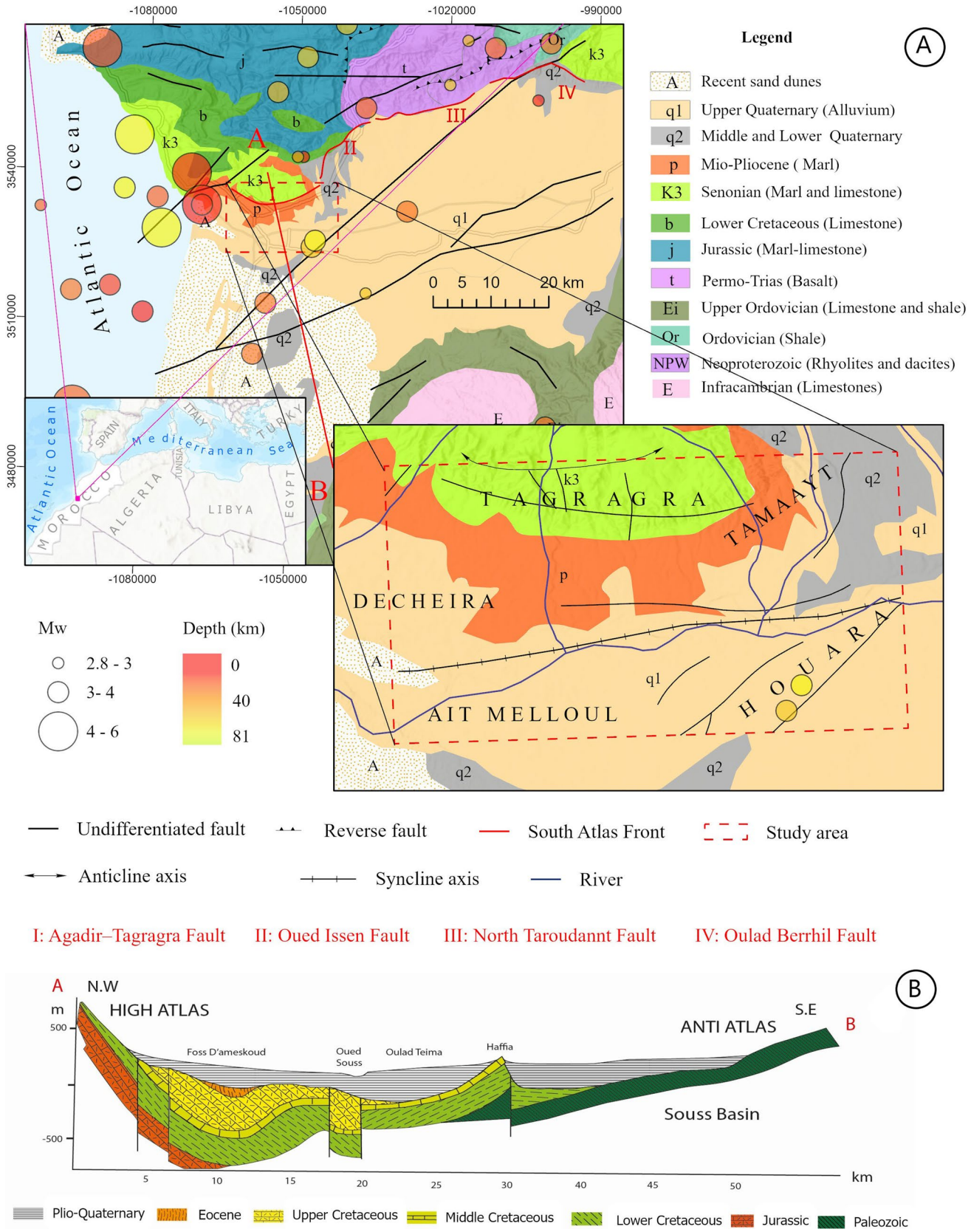

Fig. 1 Geological and seismotectonic context of the study area. **A** geological map and earthquakes occurring in the Souss basin, **B** a cross-section of the Souss basin (Ambroggi 1963)

Oued Issen Fault oriented WSW-ENE, the 45-km long North Taroudannt Fault-oriented E-W, and the 40-km long Oulad Berrhil Fault oriented E-W to WNW -ESE (Sébrier et al. 2006) (Fig. 1). The 1731 Santa Cruz earthquake of IX intensity was the first historically reported earthquake (El Mrabet 2005). The 1755 Lisbon earthquake (VIII intensity) caused catastrophic damage in several Moroccan coastal cities (Silva et al. 2021). The 1960 Agadir earthquake (Mw = 5.9) claimed over 12,000 lives and destroyed over 75% of the city (Cherkaoui and Hassani 2012). Recently, the 2023 Al-Haouez earthquake, considered the most powerful historical earthquake to strike Morocco with a magnitude of 6.8, caused catastrophic damage within a 50 km epicenter radius and claimed over 2946 lives (Khadrouf et al. 2024).

3 Data and methodology

Most engineering projects require data on subsurface layers to a maximum depth of approximately 30 m below the ground surface. This depth was reached mainly using the most common geophysical methods. This study delineated the main geological engineering units using geological investigations and the ERT method. The ERT method was used as a quick and accurate method to depict the vertical distribution of subsurface layers, thereby delineating the primary engineering units. These units were subsequently characterized by quantifying their elastic-dynamic, geotechnical, and petrophysical parameters. The geotechnical properties include rock quality designation (RQD), ultimate bearing capacity (Q_{ult}), and seismic site classes based on V_{s30}. The petrophysical properties include density (ρ) and porosity (ϕ), V_P/V_S ratio, while the elastic-dynamic properties include Poisson's ratio (σ), bulk modulus (K), and shear modulus (μ). For this purpose, P-wave and S-wave velocities were obtained from the SRT and MASW, respectively (Fig. 2). These seismic waves were used to estimate the above properties using the parameters listed in Table 1. Finally, the results were combined and analyzed to create a final geotechnical zoning map of the study area (Fig. 3).

3.1 Geological investigations, in-situ and laboratory testing

Sixty field observations were conducted to meticulously identify, characterize, and categorize geological materials to delineate the main engineering geological units of the

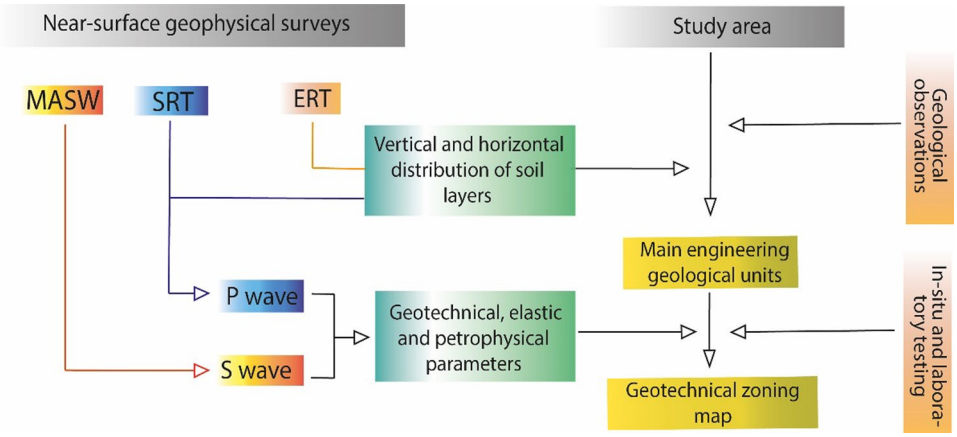

Fig. 2 Flowchart of the methodology used in this study

Table 1 Definition of parameters used in this work

Parameter	Equation	References
Density (ρ)	$\rho = 0.31 * V_p^{0.25}$	Gardner et al. (1974)
Porosity (ϕ)	$\phi = -0.175 \ln(V_p) + 1.65$	Watkins et al. (1972)
Shear modulus (μ)	$\mu = \rho V_s^2$	Toksoz et al. (1976)
Poisson's ratio (σ)	$\sigma = \left(1 - 2\left(\frac{V_s^2}{V_p^2}\right)\right) / 2\left(1 - \left(\frac{V_s^2}{V_p^2}\right)\right)$	Telford et al. (1976)
Bulk modulus (K)	$K = \rho\left(V_{p:}^2 - \frac{3V_s}{4}\right)$	Mott et al. (2008)
Rock quality designation (RQD)	$V_p = 21.951 * \mathrm{RQD} + 0.1368$	Castagna et al. (1985)
Ultimate bearing capacity (Q_{ult})	$Q_{ult} = 10^{2.932(\log V_s - 1.45)}$	Parry (1977)
Average shear wave velocity of the upper 30 m (V_{s30})	$V_{s30} = \frac{30}{\sum_{i=1}^{N}\left(\frac{n_i}{c_i}\right)}$	Abudeif et al. (2019)

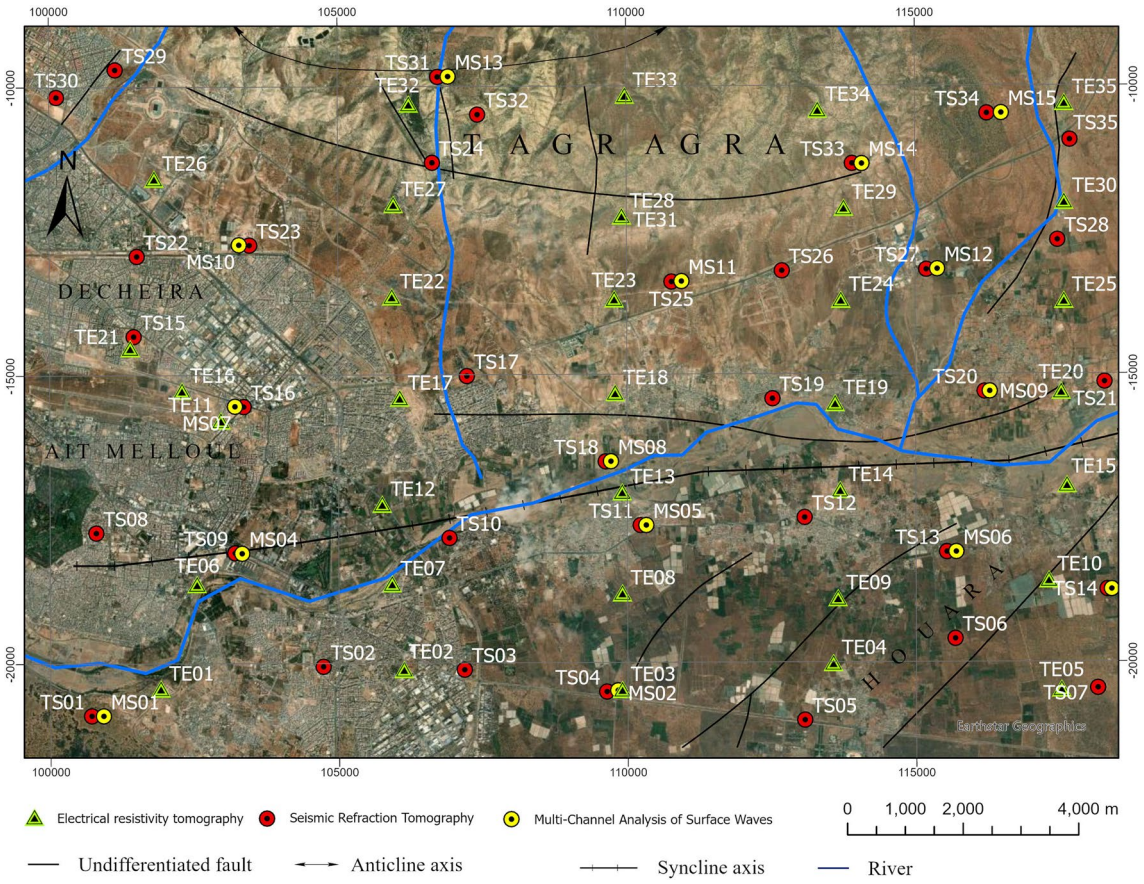

Fig. 3 Satellite image of the study area showing the ERT, SRT, and MASW profile distributions

study area. The characterization methods and classification schemes advocated by Tálita De Sena Nola and Zuquette (2021) were methodically adopted, encompassing lithological diversity, degree of weathering, the origin of materials (anthropogenic, natural, or transported), material strength, and mechanical discontinuities. In-situ investigations were performed using coring boreholes and trial pits. Representative soil and rock samples were collected and stored in polyethylene bags. Few tests have been conducted on rock samples, including rock quality designation (RQD), porosity, and rock density. Classification tests, such as grain-size analysis, Atterberg's limits, moisture content, methylene blue test (VBS), and dry bulk density, were performed on the soil samples to determine their geotechnical properties. The rock and soil tests were conducted in accordance with Moroccan standards.

3.2 2D ERT technique

To estimate the apparent resistivity of the subsurface and illustrate the vertical and horizontal variations in the soil units, 25 ERT survey lines were carried out in the study area (Fig. 3). The electrical resistivity data were obtained using an ABEM Terrameter LS2 resistivity meter equipped with 64 steel electrodes. The electrode distances were set to 2.5 m, giving a profile length of 157.5 m for all the measurement sites. The Wenner-Schlumberger array (Loke and Barker 1996; Dahlin and Loke 1998) was employed for its capability to achieve detailed models of both lateral and vertical resistivity variations allowing the mapping of horizontal and vertical geological structures with high sensitivity (Akingboye 2023). Basic quality control procedures were implemented using x2ipi software. Erroneous measurement points were manually eliminated (Fig. 4A). The obtained data were then processed using the RES2DINV inversion software employing the least-squares algorithm (Loke 2004) (Fig. 4B). Moreover, different damping values were applied to enhance the inversion, depending on the noise level in the data. The resolution of the resulting 2-D resistivity model depends on the distribution and number of acquired data points. The penetration depth varied between 25 and 30 m.

3.3 SRT technique

The distribution of P-wave velocities in the study area was calculated from 33 profiles using the SRT procedure

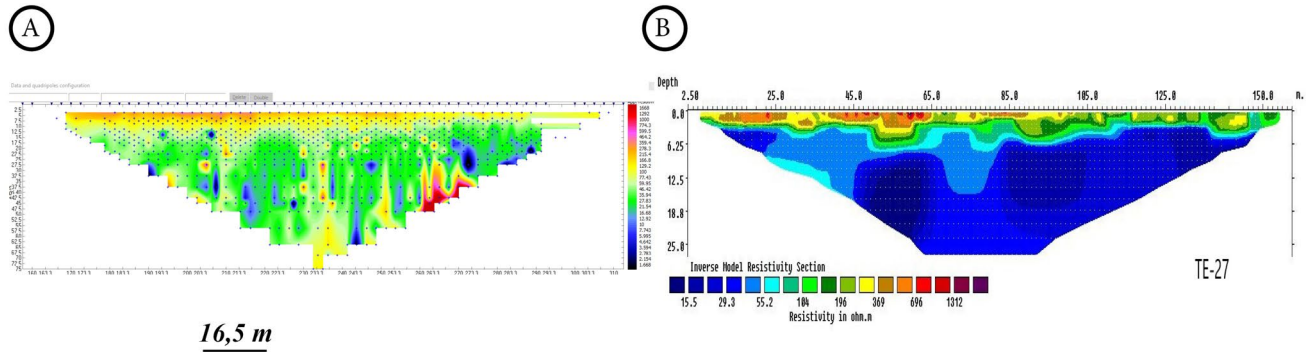

Fig. 4 Example of ERT analysis. **A** ERT data points in X2ipi software at TE-27, and **B** electrical resistivity model at profile TE-27

(Fig. 3). Data were acquired using a 24-channel seismograph (ABEM TERRALOC Pro 2) with 4.5 Hz vertical geophones at a 5m offset. A 10 kg sledgehammer striking an iron plate vertically served as a seismic source for implementing an acquisition system for forward, inline, midpoint, and reverse shooting. Raw data were processed using SeisImager/2D software (Fig. 5A, B). The processing involves a modeling technique that addresses the subsoil as a continuous medium and divides it into discrete cells, each characterized by a consistent P-wave velocity value. Using the forward modeling approach, iterative ray tracing was conducted between the source points and receivers within the presumed model. The algorithm continuously assesses the agreement between the computed and observed travel times to enhance the model's accuracy. This iterative process persists until the accepted root-mean-square (RMS) error between the observed and calculated travel times is obtained (Pegah and Liu 2016).

3.4 MASW technique

One of the widely used methods for estimating the S-wave velocity of the subsoil is the utilization of the dispersion characteristics of Rayleigh-type surface waves. Therefore, the active source MASW method was employed. Fifteen 1D-MASW lines were used at the same location as the SRT lines to calculate the soil elastic properties (Fig. 3). The study employed the MASW technique using a 24-channel seismograph model ABEM equipped with low-frequency geophones (4.5 Hz) and powered by a 12 V battery. The profiles were 69 m long with a geophone spacing of 3 m. A 10 kg sledgehammer was used as the source. Data were acquired at a sampling interval of 0.5 ms and a record length of 1 s for forward, center, and reverse shots. The forward and reverse shots had a 3 m offset, supplemented by an additional central shot at the profile's midpoint. The dispersion characteristics and inversion analysis of the raw data were performed using SeisImager software. The data were transformed in the frequency domain, and by tracing the high-energy concentration, the phase-velocity dispersion curve was obtained (Fig. 6A). The 1D shear-wave velocity models were calculated by applying a least-squares inversion algorithm (Fig. 6B).

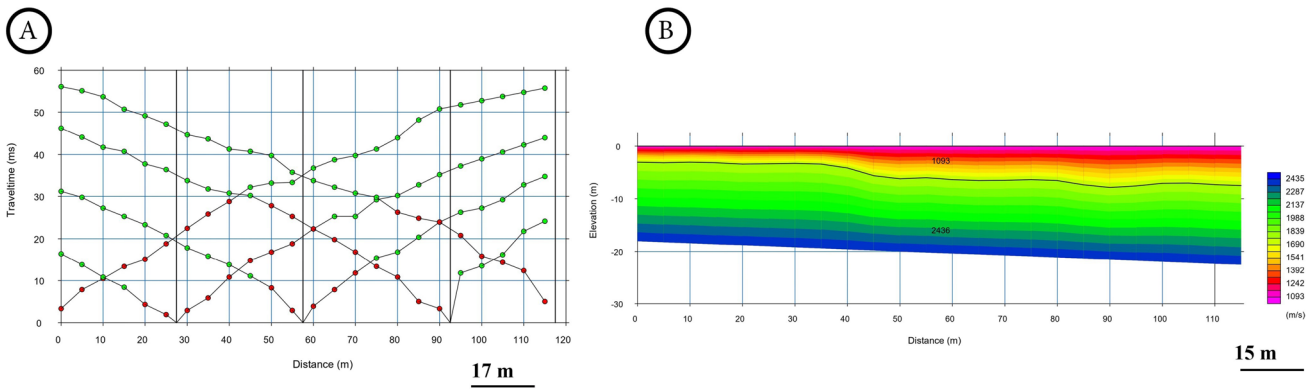

Fig. 5 Example of SRT analysis. **A** Time distance curves, and **B** velocity-depth model

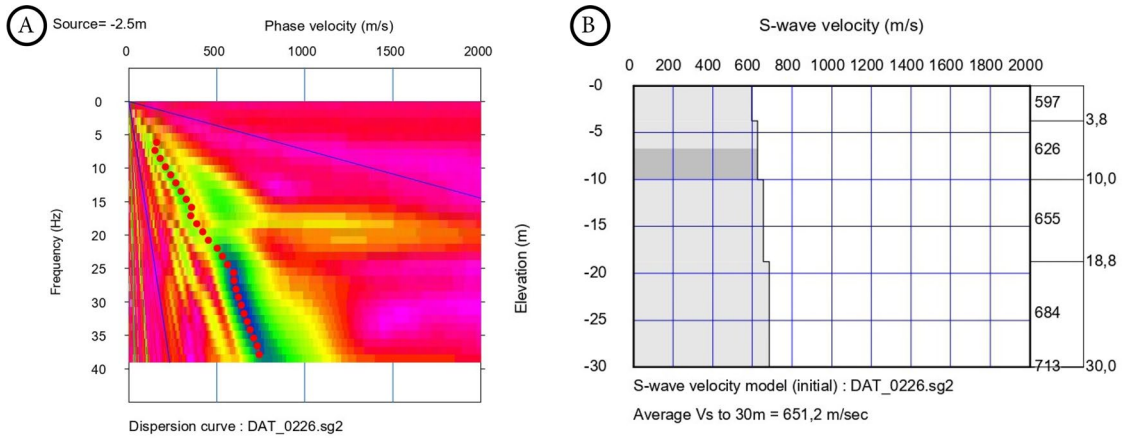

Fig. 6 Example of MASW analysis. **A** Frequency versus phase velocity, and **B** 1D-VS model

4 Results and discussion

4.1 Geological investigations, ERT imaging, and identification of geotechnical units

The main geological engineering units were delineated by combining surface geological observations, drilling cores, trial pits, and 2D ERT models (Fig. 7). The field surveys' results revealed the presence of five main subsurface engineering units: the Tagragra's Dome, recent alluvial fans, cemented alluvial fans, floodplain, alluvial terrace, limestone plateau, and sand dune.

The dome consists of alternating limestone or sandy limestone and marl and/or a thick layer of marly limestone. Field rock strength and weathering analyses (GCO 1988; BSI 2003) reveal a weak rock partially weathered in the marl and marly limestone layers but hard and unweathered rock in the sandstone limestone layers. These geotechnical properties are consistent with the RQD values ranging between 80 and 100%. The rock density (ρ), dry specific weight (γd), and water content (w) are between 1.55 and 2.64 g/cm^2, 16.1–19.8 kN/m^2, and 3.5–12%, respectively. Two main geoelectrical layers were identified by comparing the results of the 2D-ERT sections, boreholes, and trial pits conducted in this area. The first layer is an undeveloped soil, ranging from 20 cm to 1 m in thickness, formed from debris and weathering of marl and limestone. The apparent resistivity of this layer was relatively high and varied between 84 and 1970 Ohm m. The second layer exhibits low resistivity values ranging between 7 and 55 Ohm m, with a thickness of approximately 24 m. These values reflect the presence of relatively dry limestone or dry marly limestone. This interpretation was substantiated by water content measurements at depths greater than 2 m, ranging from 6.3 to 12% (Fig. 7A).

The alluvial fans area mainly comprises two geomorphological units (recent and old cemented alluvial deposits). The recent alluvial fan unit is composed of heterogeneous sediment accumulations such as dolomitic limestone, reworked limestone, alluvial conglomerates, consolidated conglomerates, interceded coarse-grained limestone, and conglomerates. The floodplain area is generally formed by homogenous sediments, such as lacustrine and nodular limestone, overlain by silt or colluvial deposits. Grain-size analysis revealed that the fine particle elements (< 80 µm) were between 9 and 78%, sands (0.05–2 mm) were between 12 and 20%, and gravel (> 20 mm) was 3 and 25%, respectively. These results indicate gravelly loam (soil composed mostly of sand, silt, and a smaller amount of clay), sandy loam, silt, and silty loam. The plasticity index values were between 9 and 12%, indicating medium plastic soil. The water content (w), dry specific weight (γd), specific weight (γh), and VBS are between 3.5 and 10.5%, 15.5–17.1 kN/m^2, 16.4–17.7 kN/m^2, and 2.1–3.3, respectively. Most 2D-ERT models obtained within the alluvial fan zone showed several resistivity anomalies indicative of complex lithological characteristics. These anomalies also reveal heterogeneous geometries in both vertical and horizontal directions. Zones characterized by high resistivity values (> 300 Ohm m) are primarily linked to cemented and low porosity facies such as conglomerates, dolomitic limestone, and silt. Low to moderate resistivity values (< 200 Ohm m) were interpreted as unconsolidated deposits such as reworked limestone, alluvial conglomerates, and/or coarse-grained limestone. Conversely, the floodplain area exhibits a layered geometry, where the resistivity values decrease vertically from the surface to the depth. Most profiles in this area show two geoelectric zones, where the resistivity values in the first zone range between 23 and 179 Ohm m, and in the second zone between 5 and 60 Ohm m. The first zone (1–3

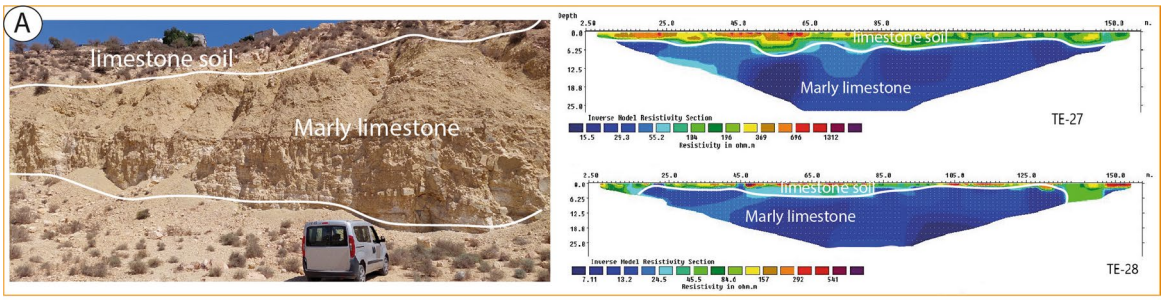
A
limestone soil
Marly limestone
limestone soil
Marly limestone
TE-27
limestone soil
Marly limestone
TE-28

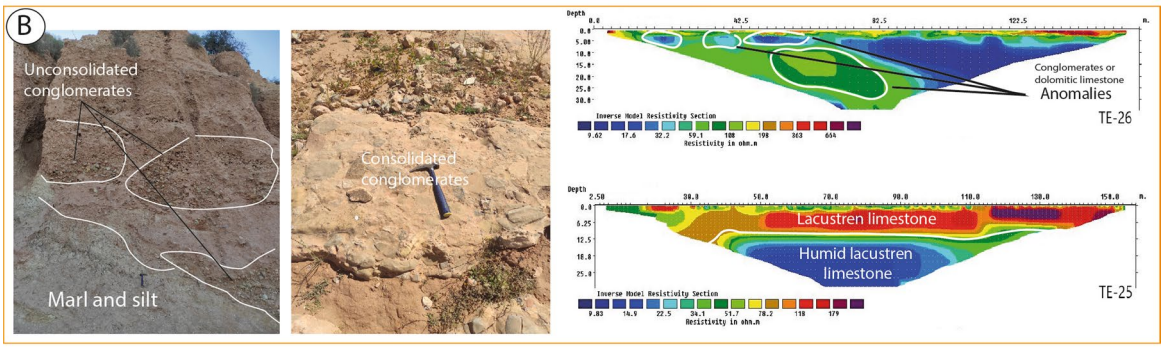
B
Unconsolidated conglomerates
Marl and silt
Consolidated conglomerates
Conglomerates or dolomitic limestone
Anomalies
TE-26
Lacustren limestone
Humid lacustren limestone
TE-25

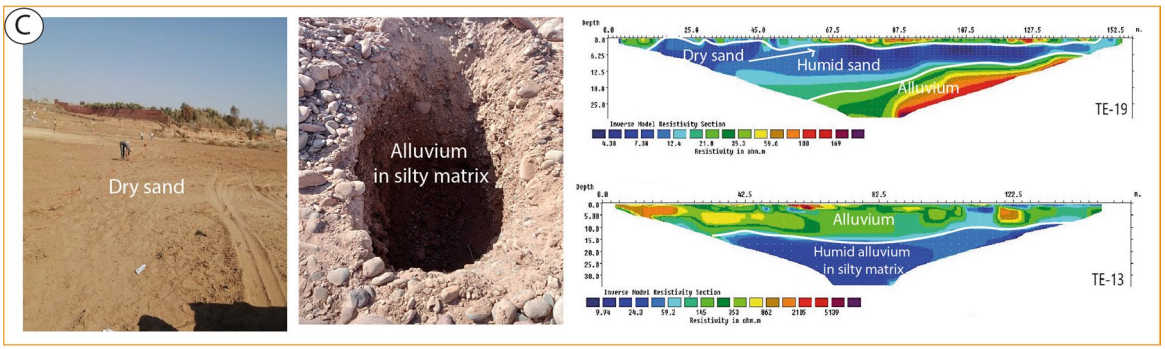
C
Dry sand
Alluvium in silty matrix
Dry sand
Humid sand
Alluvium
TE-19
Alluvium
Humid alluvium in silty matrix
TE-13

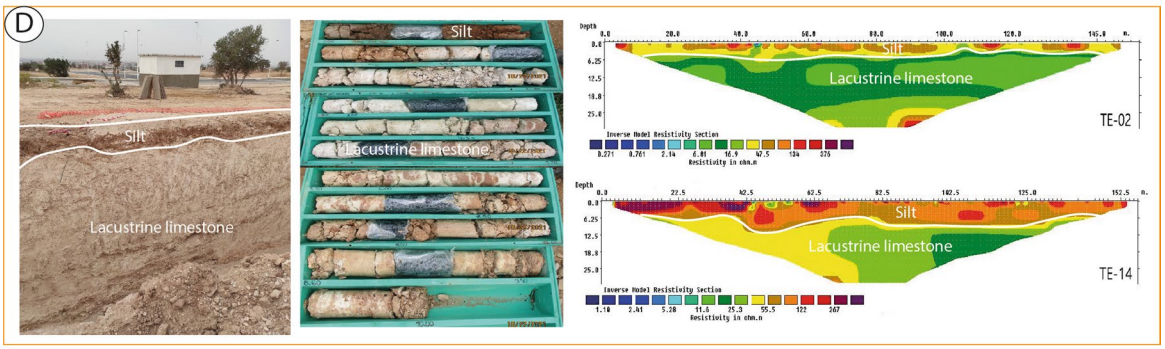
D
Silt
Lacustrine limestone
Silt
Lacustrine limestone
Silt
Lacustrine limestone
TE-02
Silt
Lacustrine limestone
TE-14


E
Consolidated Sand
Sand
Silt
Sand dunes

◂**Fig. 7** Representative 2D-ERT models correlated with the nearest geological and geotechnical investigations. **A** Tagragra's Dome, **B** Recent and old alluvial fans unit, **C** alluvial terraces unit, **D** limestone plateau unit, and **E** sand dune unit

m) is attributed to silt or dry lacustrine limestone, while the second zone (21–24 m) is relatively humid lacustrine limestone (Fig. 7B).

Alluvial terraces consist of silts, sandy silts, clayey silts, interceded silts, and pebbles. Chanel sediments consist of recent pebbles of a silty sand matrix. Fine elements (< 80 µm) were between 22 and 97%, sands (> 2 mm) were between 18 and 89%, and gravels (> 20 mm) were 2 and 42%, respectively. Almost all samples showed no measurable plasticity, which can be explained by the high proportions of silt and sand. The water content (w), dry specific weight (γd), specific weight (γh), and VBS are between 1.3 and 17.7%, 13.7–24.3 kN/m^2, 14.1–25 kN/m^2, and 0.12–3, respectively. Interpretation of the 2D-ERT sections based on borehole data revealed two or three geoelectric layers depending on the locations of the ERT lines. Profiles with two geoelectric layers indicate sandy silt overlying the silt. Alternatively, they may reveal homogenous sandy silt (or pebbles in the channel bed) with increased moisture content from the surface to the depth. The first layers had thicknesses varying from 10 to 12 m and a resistivity value between 107 and 956 Ohm m. The second layers had a resistivity value between 7 and 285 Ohm m. Profiles with three geoelectric layers indicate silt or sandy silt interbedded with pebbles (Fig. 7C).

The limestone plateau consists of limestone debris, limestone, or sandy limestone, overlain by a thin layer of silt. Laboratory tests on silt samples revealed that the water content (w), VBS, plasticity index, dry specific weight (γd), and specific weight (γh) are between 10 and 18%, 2–4.2, 12–24, 16.2–18 kN/m^2, and 16–19 kN/m^2, respectively. Samples from limestone revealed that rock porosity, density, and water content (w) were between 8.3%-23.5%, 2.1–2.4, and 11–14, respectively. Based on the 2D-ERT profiles and boreholes conducted in this unit, two geoelectric layers are differentiated: the first layers are silt or weathered limestone (with a thickness between 1 and 1.5 m) characterized by high to medium resistivity values ranging between 47 and 1019 Ohm m. The second layer is limestone or sandy limestone characterized by low to moderate resistivity values (ranging from 6 to 148 Ohm m) and thicknesses ranging from 24 to 23 m (Fig. 7D).

According to borehole BH01, the dune unit consists of aeolian sand and silty sand (5 m) overlying silt deposits (> 5 m). The physical properties of the sand layers, such as water content (w), dry specific weight (γd), and specific weight (γh), fall within the ranges of 5–11%, 19.5–19.7 kN/m^2, and 18–18.8 kN/m^2, respectively. The results of the VBS (0.2), plasticity index (not measurable), and sand equivalents (92%) indicate that the sand is clean and non-plastic. Samples from silt layers indicate that fine elements (< 80 µm), sand (0.05–2 mm), and gravel (> 20 mm) range from 80 to 98%, 2–3%, and 1–13%, respectively. The water content (w), dry unit weight (γd), and specific weight (γh) range from 3.5 to 22%, 15.2–22.2 kN/m^2, and 18.5–23 kN/m^2, respectively. The plasticity index (11–20%) and VBS (5,2) revealed medium to high plastic clayey silt. ERT surveys were not conducted in this unit (Fig. 7E).

4.2 S and P wave velocities

S-wave velocities (V_s) were determined from 15 1D-MASW profiles conducted across engineering geological units. These profiles were executed at the same sites investigated by the 2D-SRT survey. The reaching depths of the 1D-MASW and 2D-SRT were 30 and 20 m, respectively. Thirty-three 2D-SRT profiles were obtained, particularly in areas with scarce geotechnical data. After the data analysis, S- and P-wave velocity maps were prepared using the inverse distance to a power gridding method. As shown in Fig. 8A, B, the V_s values ranged between 160 and 1200 m/s, and the V_p values ranged between 382 and 3700 m/s respectively. The surveyed 1D-MASW profiles showed a slight progressive increase in V_s with depth, whereas the 2D-SRT profiles exhibited a significant increase in V_p with depth. This difference in velocity between the P- and S-waves was primarily attributed to variations in soil porosity. Generally, three geoseismic layers were identified, depending on V_s and V_p variations.

The first geoseismic layer is a surface layer corresponding to silt, sand, weathered limestone, weathered marl, conglomerate, colluvial, and alluvial deposits. Its thickness varies between 1 and 6 m, and its V_s and V_p values range from 160 to 680 m/s and 382–3757 m/s, respectively. Low velocities mainly correspond to unconsolidated deposits, whereas high velocities are attributed to compact deposits. Data from geological surveys, boreholes, and trial pits support these results. Both seismic and geoinvestigations have highlighted surface lithological heterogeneity.

The second geoseismic layer has relatively higher seismic velocities than the first; its V_s and V_p velocities vary between 215 m/s and 805 m/s and 432 m/s and 3494 m/s, respectively. These values indicate the presence of dense to medium-dense soil and rock deposits, including limestone and marly limestone in the Tagragra's Dome, limestone sandstone on the limestone plateau, and compacted alluvial sediment in the Oued Souss channel bed. In contrast, areas with low seismic velocities revealed unconsolidated and fine-grained deposits, such as silts found in borehole BH1 drilled within the sand dune area.

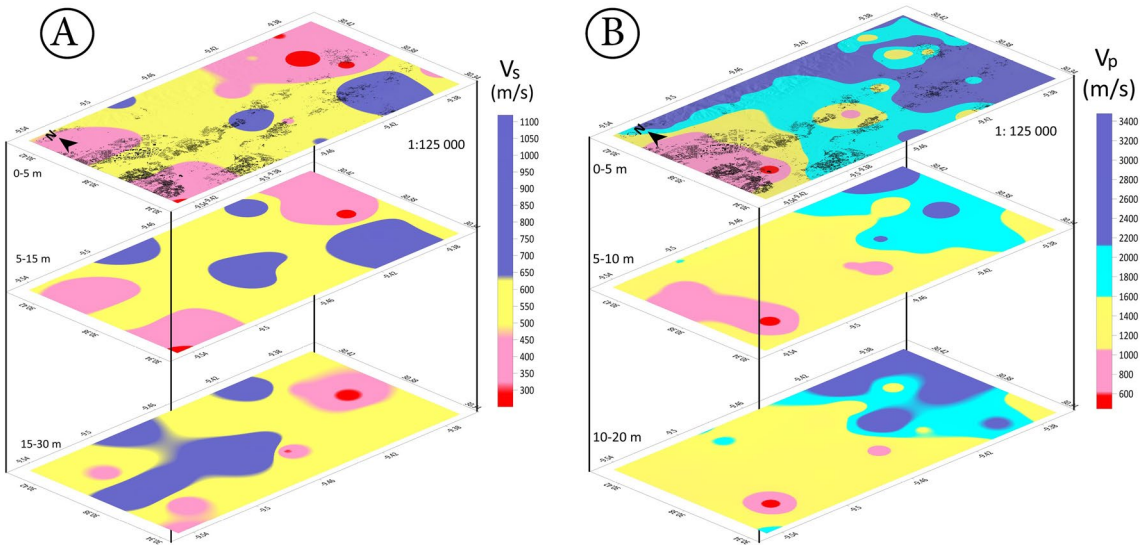

Fig. 8. 3D perspective view of the maps depicting the velocities of **A** V_s-waves and **B** V_p-waves

The third geoseismic layer has V_s values between 300 and 1120 m/s and V_p values between 456 m/s and 3764 m/s. According to the Moroccan seismic building code (RPS 2011), the layer can be classified as bedrock when the V_s velocities in a geoseismic layer reach values greater than 760 m/s. Layers with V_s velocities between 400 and 760 m/s are classified as very dense soils or fractured weathered rock, whereas deposits with lower velocities (< 150 m/s) are soft soils. Generally, the V_p velocities obtained in the third layer show relatively high values (1200–3400 m/s). By combining the above-mentioned P- and S-wave velocity distributions and borehole data, zones with high velocities ($V_s > 700$ m/s and $V_p > 1800$ m/s) were interpreted as limestone rocks, marly limestone rocks, sandstone limestone rocks, and compacted conglomerates. Zones with moderate velocities (V_s between 700 and 400 m/s and V_p between 1800 and 1400 m/s) revealed limestone rocks, weathered limestone sandstone, and medium-compacted conglomerates, while zones with low velocities ($V_s < 400$ m/s and $V_p < 1400$ m/s) revealed silt or sand.

4.3 Geotechnical, elastic, and petrophysical properties

The calculated P- and S-wave velocities obtained from SRT and MASW surveys were used to estimate the geotechnical, elastic, and petrophysical properties of the subsoils. Several maps were generated using data calculated from the geotechnical engineering parameters listed in Table 1. The seismic and engineering results are listed in Supplementary data.

4.3.1 Q_{ult}, RQD, and V_{S30}

Q_{ult} represents the bearing stress that causes the shear failure and settlement of the foundation. The Q_{ult} map of the study area showed three layers (0 to − 5 m, − 10 m, and − 10 to − 20 m) (Fig. 9A). The first layer showed values between 16.3 and 1131 kN/m^2. The second and third layers show relatively medium values ranging between 38.7 and 1856.5 kN/m^2 and 60.2–4849 kN/m^2, respectively. The extended gap between these values highlights soil heterogeneity and weak competence of the first layer.

The RQD test measures the extent of fractures and joints in a 1-m core rock sample. Typically, high RQD values indicate solid and unaltered rocks, whereas low values indicate fractured and weathered rocks. The RQD map shows three layers (Fig. 9B). The first layer (0–5 m) exhibits mainly low RQD values between 20 and 45%, indicating very poor to poor rock quality. Medium-to-high values were also observed in the eastern part of the study area. The second and third layers show high RQD values ranging between 40 and 100%, indicating fair to excellent-quality rocks.

V_{S30} plays a crucial role in site characterization and earthquake engineering. This parameter is a fundamental indicator of soil stiffness, which influences ground motion amplification and the response of structures during earthquakes. The results for V_{S30} ranged between 179 and 830 m/s. According to (Eurocode 8 2005) classification, the study area is classified into three classes: site Class B, located in most parts of the study area, and the rest of the sites are classified as site Classes C and A (Fig. 9C).

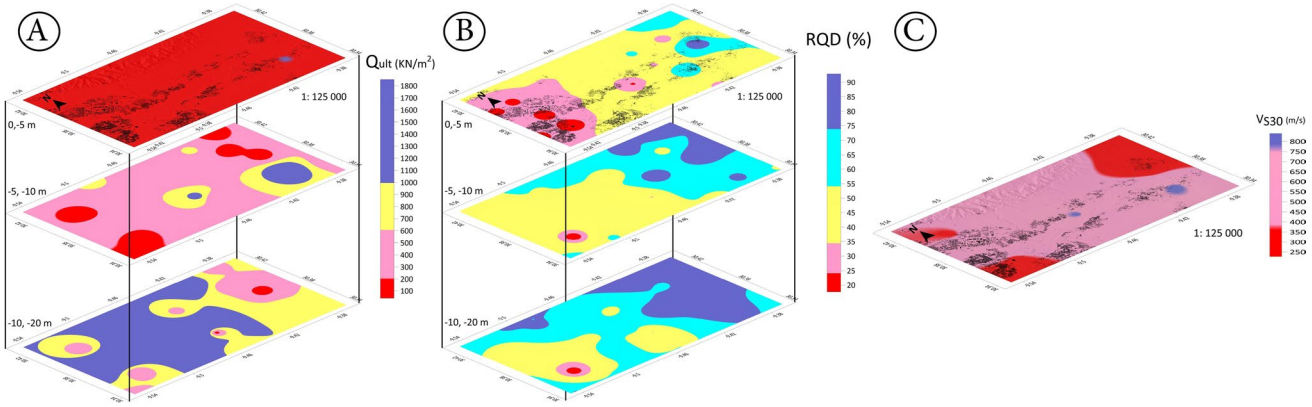

Fig. 9. 3D perspective view of the maps depicting **A** ultimate bearing capacity (Q_{ult}), **B** rock quality designation (RQD), and **C** seismic site classes based on V_{s30}

4.3.2 Density (ρ), Porosity (ϕ), and V_P/V_S ratio

The petrophysical properties of the three layers are outlined as follows.

1. Density: The estimated density values for the first layer range between 1.37 g/cm^3 and 2.42 g/cm^3. Low values were located in the western part of the study area and some parts of the cemented alluvial fans area. The second and third layers show relatively high and homogeneous densities ranging between 1.50 and 2.20 g/cm^3 (Fig. 10A).
2. The first layer's porosity ranges between 28 and 60%. This layer shows relatively high porosity values, attributed to unconsolidated rocks and soils such as sand, silt, weathered limestone, and marlstone. The porosities of the second and third layers show relatively medium and homogeneous values, ranging between 32 and 44% (Fig. 10B).
3. The saturation of pores in soil layers can be assessed by calculating the VP/VS ratio. This is possible because P wave velocities are sensitive to the type of pore saturation (water or gas), whereas S waves, traveling solely through solids, remain unaffected (Uyanık 2019). Soil layers with a V_p/V_s ratio of around 1.5 indicate a porous or air-filled medium. At the same time, values greater than 4 suggest a water-saturated medium (Uyanık 2011)—values of this ratio in the first layer range between 0.6 and 10. The western part shows relatively consistent values around 1.5, which suggests that the soil in this area is porous and air-fille. The second and third layers show values between 1 and 10. However, the distribution of these values is generally around 4, suggesting a less porous or more water-saturated medium (Fig. 10C).

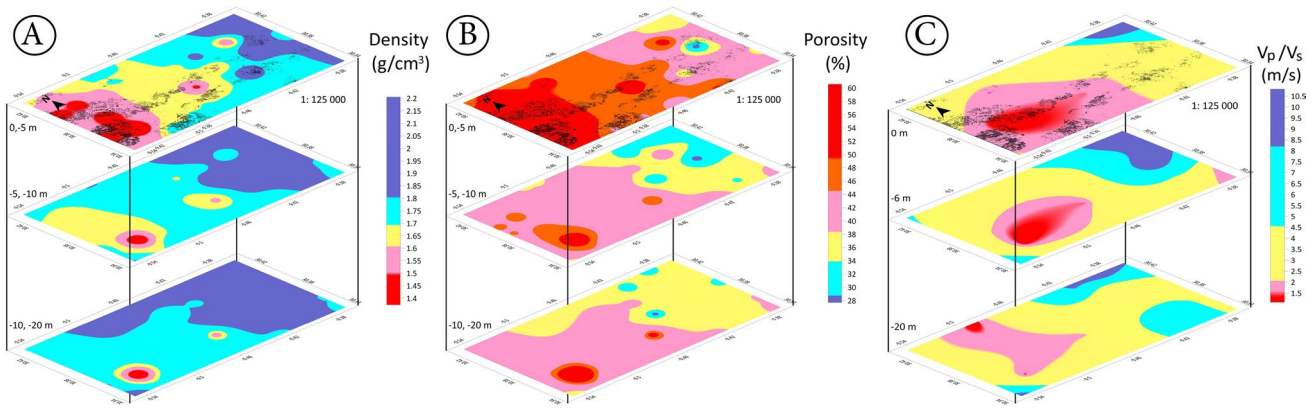

Fig. 10. 3D perspective view of maps illustrating **A** density (ρ), **B** porosity (ϕ), and **C** V_p/V_s ratio

4.3.3 Poisson's ratio, shear modulus, and bulk modulus

The resulting maps of the elastic moduli for the three layers are summarized as follows:

1. Poisson's ratio is a key parameter that describes how materials respond to deformation. This ratio spans from 0.0 in hard rocks to 0.20–0.45 in clays and silts and can reach 0.5 in loose soil. Generally, materials with lower strength exhibit higher Poisson's ratios, whereas the opposite holds true for stronger materials. In this study, the Poisson's ratio (σ) values of the first layer range between 0 and 1.97, while the second and third layers show relatively homogeneous values, ranging from 0 to 0.3. The northeastern part of the study area showed high values, ranging between 1 and 1.97 (Fig. 11A).
2. The shear modulus, also known as the rigidity modulus (μ), is a fundamental material property used to describe the stiffness of a material subjected to shearing forces. The values for the first layer range between 1.26E+06 and 9.80E+05, while the second layer's range is between 8.92E+05 and 1.20E+07. The third layer exhibits relatively high rigidity values, ranging from 1.12E+06 to 2.74E+07, indicating the presence of condensed soils (Fig. 11B).
3. The bulk modulus of the first layer varied between (1.96E+03) and (3.36E+05) dyne/cm^2. These results indicate that the soil in the top layer is weak and very weathered. The second and third layers vary from (2.85E+05) to (3.03E+03) dyne/cm^2 and (2.29E+05) to (3.40E+03) dyne/cm^2, respectively (Fig. 11C). Compared to the first layer, these results indicate that the soil in the second and third layers is moderately weathered with competent geotechnical properties.

4.3.4 Geotechnical zoning map

Geotechnical engineering is based on studying the intrinsic properties of subsoil to minimize complexity and heterogeneities. Therefore, quantifying and categorizing uncertainties is crucial for successful engineering design (Shang et al. 2021). Technical tools such as geophysical methods and geotechnical maps are essential. The geotechnical zoning map was created by combining data from field surveys, including laboratory measurements, geological observations, ERT survey results, and parameters derived from the S-wave and P-wave velocities. The minimum and maximum values of the engineering and geotechnical parameters were determined (from the three subsurface geoseismic layers) for each unit (Fig. 12). Examination of the results revealed soil diversity in the horizontal and vertical directions. Soil competency increased with depth in all seismic profiles due to the compaction and cementation processes. Furthermore, seismic wave propagation at very low strain levels in soil layers validates using the elasticity theory for measuring dynamic soil properties. In this case, the soil response should be linear; however, at moderate to large strain levels, this response starts to be nonlinear. Therefore, it is recommended that findings from seismic waves be integrated with laboratory measurements (Al-Heety et al. 2021). Analysis of the results reveals that the geomorphological forms of the study area strongly influence the delineated zone units. For example, alluvial fans are characterized by various parameters influencing soil quality, such as sediment composition, grain size distribution, degree of saturation, and cementation. Terrace and dune sediments consist of finer, less consolidated, and less cohesive material. Plateau and dome sediments are primarily homogeneous and exhibit low heterogeneity. Therefore, a multidisciplinary approach integrating geological, geomorphological, and geophysical investigations is crucial for comprehensive soil characterization and mapping. The evaluation of the study site's suitability

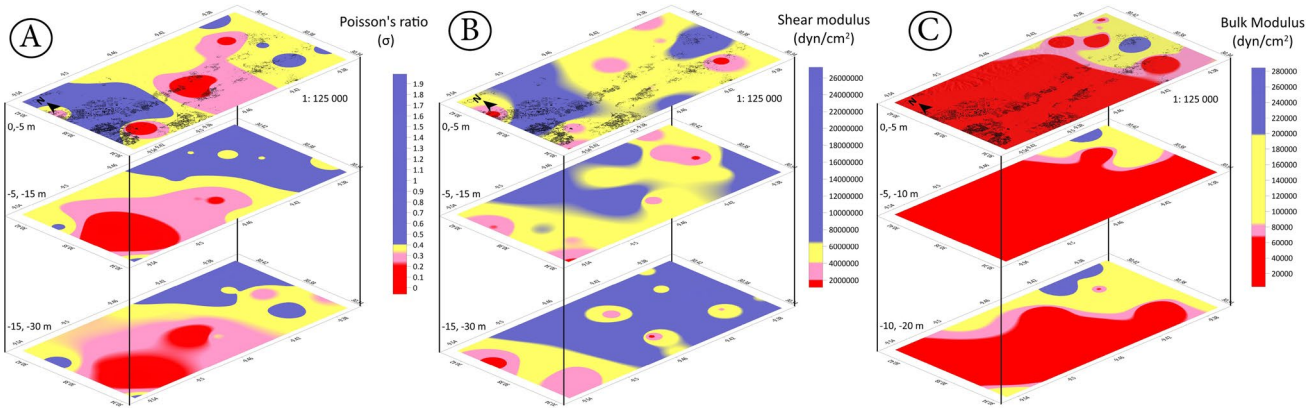

Fig. 11. 3D perspective view of the maps depicting 3D illustration maps: **A** Poisson's ratio (σ), **B** shear modulus (μ), and **C** bulk modulus (K)

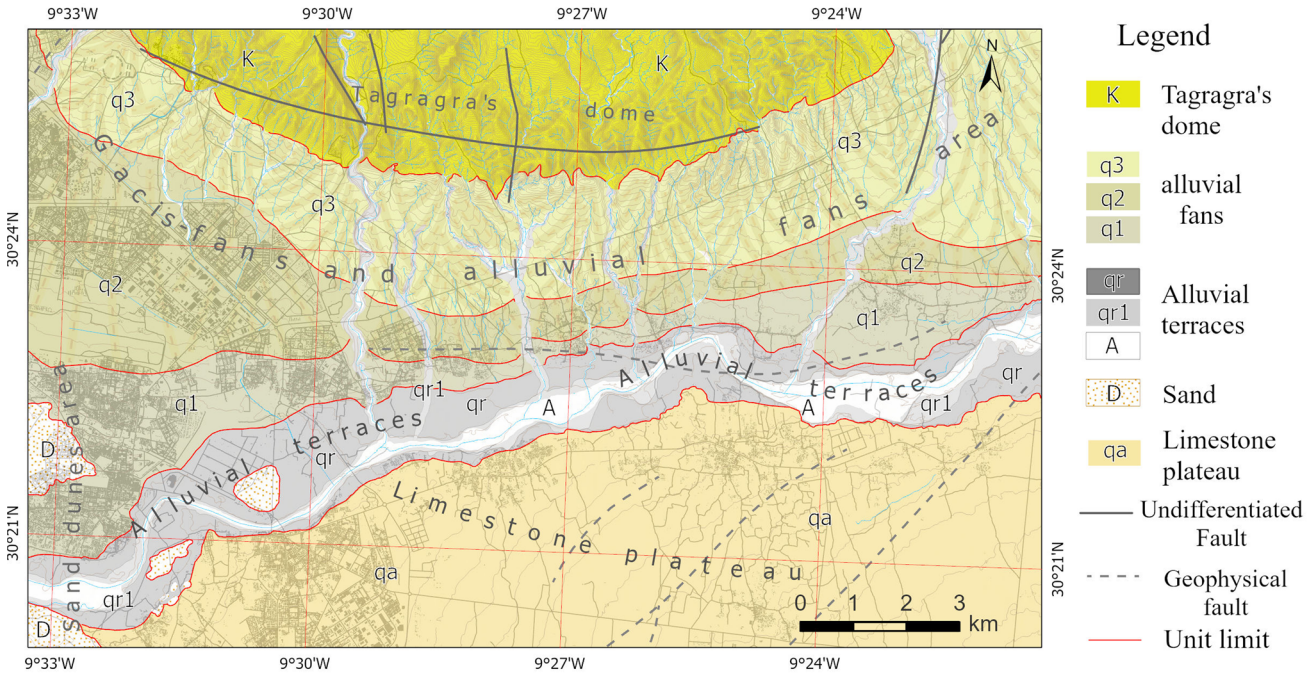

Unit	Sub-unit	Lithology	Density (kN/m3)	Porosity (%)	RQD (%)	Qult (kN/m2)	EC8 classification	Poisson's Ratio	Shear Modulus	Bulk Modulus (dyne/cm2)
Tagragra's Dome (K)		Limestone, sandstone and marl	15.14 23.80	21 54	36 100	107 1705	B	2,00E+00 4,96E-01	9,52E+ 05 1,39E+ 07	1,51E+ 04 3,36E+ 05
Alluvial fans	Recent alluvial fans (q3)	Limestone, silt, and conglomerates	15.02 19.40	35 48	27 75	16 473	B and C	4,06E- 01 2,01E- 01	9,54E+ 05 2,72E+ 06	5,33E+ 03 5,33E+ 04
	Old alluvial-fans (q1 and q2)	Limestone, silt, colluvial deposits	14.09 21.80	27 58	21 100	26 3455	B	-6,24E- 02 4,44E- 01	5,14E+ 05 2,74E+ 07	2,99E+ 03 1,52E+ 05
Alluvial terraces	Recent terraces (qr1 and qa)	Silt, sandy silt, clayey silt, alluvium	16.73 19.45	38 70	38 70	-	-	-	-	-
	Fossil terraces (qr)	Limestone, silt and sandy silt	13.44 24.80	21 58	17 100	75 4889	C and A	-6,11E- 02 2,80E- 03	9,80E+ 05 1,85E+ 07	1,96E+ 03 3,18E+ 04
Sand dunes (D)		Sand	15.46 21.30	29 57	21 73	23 213	C	3,96E- 01 4,74E- 01	8,92E+ 05 3,16E+ 06	6,90E+ 03 1,24E+ 05
Limestone plateau (qa)		Limestone, sandstone	15.60 21.70	29 52	29 100	280 805	A and B	1,86E- 01 4,60E- 01	1,35E+ 06 1,20E+ 07	3,03E+ 03 8,05E+ 04

Fig. 12 Final Geotechnical Zoning map

for construction is conducted by combining data from geological and geomorphological conditions as well as the calculated parameters. The Tagragra's Dome and the limestone plateau present fewer uncertainties and more suitable conditions. The suitability of the alluvial fan units depends on the degree of compaction and cementation. Old and cemented alluvial deposits are generally suitable, while recent alluvial deposits require additional geotechnical investigations. Alluvial terraces are moderately suitable and require advanced investigations. Furthermore, it is worth noting that these areas are susceptible to flood hazards. The sand dune unit is not suitable and is generally prone to liquefaction.

Given the urgent need to optimize the cost and efforts associated with geotechnical investigations, this study presents an integrated approach that combines geophysical, geological, and geotechnical data. This approach results in a comprehensive geotechnical zoning map, revealing the variability in soil properties and their implications for

construction suitability. This is essential for accurate soil characterization and facilitates more informed engineering decisions. Future research should focus on the entire Souss Basin, given the intense soil heterogeneities and the rapid urban development known in this region on the one hand, as well as the cost-effectiveness and reliability of these approaches on the other hand.

5 Conclusion

The eastern Agadir (Morocco) was chosen as a designated zone for urban expansion to accommodate the urban sprawl of the city, necessitating soil geotechnical characterization. Subsurface geophysical investigations are powerful, cost-effective, and rapid tools for addressing various geotechnical issues and estimating different elastic, dynamic, and geotechnical parameters of soil layers. Electrical resistivity tomography (ERT), seismic refraction tomography (SRT), and multichannel analysis of surface waves (MASW) techniques were employed, along with field and laboratory tests, to create a geotechnical zoning map of the study area.

The ERT method was used to delineate the vertical and horizontal extents of the primary engineering geological units. The results were further supported and validated using in situ identification tests. P- and S-waves were employed to estimate the essential geotechnical and elastic-dynamic moduli and petrophysical characteristics.

The seismic waves (V_P and V_S) finding indicate that the study area primarily comprised three geoseismic layers. The first geoseismic layer constitutes the surface layer, with V_S and V_P values ranging from 160 m/s to 680 m/s and 382 m/s to 3757 m/s, respectively. The second geoseismic layer underlies the first, with V_S and V_P velocities ranging from 215 to 805 m/s and 432–3494 m/s, respectively. This layer exhibited relatively higher seismic velocities than the surface layer. The third geoseismic layer is characterized by even higher competence than the layers above, with V_S values ranging from 300 m/s to 1120 m/s and V_P values ranging from 456 m/s to 3764 m/s.

The final geotechnical zoning map revealed five distinct zones: Tagragra's Dome, the alluvial fans (recent and old), the alluvial terrace, the limestone plateau, and the sand dune. The calculated parameters demonstrated soil heterogeneities in both horizontal and vertical directions. However, based on the calculated geotechnical and elastic-dynamic parameters, the competence of the second and third layers was higher than that of the first. Consequently, these layers can be considered as geotechnical bedrock.

The Vs_{30} map shows V_s values ranging from 179 to 830 m/s, classifying the study area into soil classes A (rock or other geological formations including 5 m of weak materials), B (deposits of dense sand, gravel, or stiff clay), and C (deep deposits of dense or medium-dense sand, gravel, or stiff clay), according to Eurocode 8.

The final geotechnical zoning map, created by geophysical surveys, plays a crucial role in urban planning by providing relevant information about the subsoil and locating areas prone to geotechnical problems at the study site. However, this map presents only an overview of the soil's geotechnical properties, and local soil heterogeneities are always anticipated, necessitating detailed investigations and testing tailored to the requirements of specific civil projects.

Supplementary Information The online version contains supplementary material available at https://doi.org/10.1007/s42990-024-00137-3.

Acknowledgements The authors thank the Editor in Chief, Dr. Attila Çiner, and reviewers for their time and constructive comments towards improving our manuscript.

Data availability All relevant data are provided in the supplementary file accompanying this manuscript.

Declarations

Conflict of interest The authors declare that they have no known competing financial interests or personal relationships that could have appeared to influence the work reported in this paper.

References

Abudeif AM, Fat-Helbary RE, Mohammed MA et al (2019) Geotechnical engineering evaluation of soil utilizing 2D multichannel analysis of surface waves (MASW) technique in New Akhmim city, Sohag, Upper Egypt. J Afr Earth Sc 157:103512. https://doi.org/10.1016/j.jafrearsci.2019.05.020

Aït Hssaine A, Bridgland D (2009) Pliocene-Quaternary fluvial and aeolian records in the Souss Basin, southwest Morocco: a geomorphological model. Glob Planet Change 68:288–296. https://doi.org/10.1016/j.gloplacha.2009.03.002

Akingboye AS (2023) RQD modeling using statistical-assisted SRT with compensated ERT methods: correlations between borehole-based and SRT-based RMQ models. Phys Chem Earth Parts a/b/c 131:103421. https://doi.org/10.1016/j.pce.2023.103421

Al-Heety AJR, Hassouneh M, Abdullah FM (2021) Application of MASW and ERT methods for geotechnical site characterization: a case study for roads construction and infrastructure assessment in Abu Dhabi. UAE J Appl Geophys 193:104408. https://doi.org/10.1016/j.jappgeo.2021.104408

Ambroggi R (1963) Etude géologique du versant méridional du Haut Atlas occidental et de la plaine du Souss. Ed. de la division de la géologie. Rabat

Ayele A, Woldearegay K, Meten M (2022) Multichannel analysis of surface waves (MASW) to estimate the shear wave velocity for engineering characterization of soils at Hawassa Town, Southern Ethiopia. Int J Geophys 2022:1–22. https://doi.org/10.1155/2022/7588306

Bello A, Muztaza NM, Abir IA et al (2022) Geophysical performance of subsurface characterization for site suitability in construction purpose. Phys Chem Earth Parts a/b/c 128:103296. https://doi.org/10.1016/j.pce.2022.103296

Berhane G, Walraevens K (2012) Geological and geotechnical constraints for urban planning and natural environment protection: a case study from Mekelle City, Northern Ethiopia. Environ Earth Sci. https://doi.org/10.1007/s12665-012-1963-x

Bouaakkaz B, El Morjani ZEA, Bouchaou L (2023) Social vulnerability assessment to flood hazard in Souss basin, Morocco. J Afr Earth Sci 198:104774. https://doi.org/10.1016/j.jafrearsci.2022.104774

BSI (2003) Geotechnical investigation and testing. Identification and classification of rock. British Standards Document, BS EN ISO 14689-1. https://doi.org/10.3403/03006990

Calamita G, Gallipoli MR, Gueguen E et al (2023) Integrated geophysical and geological surveys reveal new details of the large Montescaglioso (southern Italy) landslide of December 2013. Eng Geol 313:106984. https://doi.org/10.1016/j.enggeo.2023.106984

Castagna J, Batzle M, Eastwood R (1985) Relationship between compressional and shear-wave velocities in classic silicate rocks. Geophysics 50:571–581. https://doi.org/10.1190/1.1441933

Cherkaoui T-E, Hassani AE (2012) Seismicity and seismic hazard in Morocco 1901–2010, pp 45–55

Dahlin T, Loke MH (1998) Resolution of 2D Wenner resistivity imaging as assessed by numerical modelling. J Appl Geophys 38:237–249

De Sena T, Nola I, Zuquette LV (2021) Procedures of engineering geological mapping applied to urban planning in a data-scarce area: application in southern Brazil. J S Am Earth Sci 107:103141. https://doi.org/10.1016/j.jsames.2020.103141

Dewey J, Helman M, Knott S et al (1989) Kinematics of the western Mediterranean. Geol Soc Lond Spec Publ 45:265–283. https://doi.org/10.1144/GSL.SP.1989.045.01.15

El May M, Souissi D, Said HB, Dlala M (2015) Geotechnical characterization of the quaternary alluvial deposits in Tunis City (Tunisia). J Afr Earth Sc 108:89–100. https://doi.org/10.1016/j.jafrearsci.2015.05.003

El Mrabet T (2005) The great earthquakes in the Maghreb region and their consequences on man and environment. CNRS-LAG report, Rabat, Morocco **(in Arabic)**

Elmouden A, Alahiane N, Faskaoui M, El Morjani ZEA (2016) Dams siltation and soil erosion in the Souss–Massa River Basin, pp 1–26

Eurocode 8 (2005) Eurocode 8: design of structures for earthquake resistance-part 1: general rules, seismic actions and rules for buildings. European Committee for Standardization, Brussels

Failache MF, Zuquette LV (2018) Geological and geotechnical land zoning for potential Hortonian overland flow in a basin in southern Brazil. Eng Geol 246:107–122. https://doi.org/10.1016/j.enggeo.2018.09.032

Gardner GHF, Gardner LW, Gregory AR (1974) Formation velocity and density—the diagnostic basics for stratigraphic traps. Geophysics. https://doi.org/10.1190/1.1440465

GCO (1988) Guide to rock and soil descriptions (Geoguide 3). Geotechnical Control Office, Hong Kong, p 186

Hasan M, Shang Y, Meng H et al (2021) Application of electrical resistivity tomography (ERT) for rock mass quality evaluation. Sci Rep 11:23683. https://doi.org/10.1038/s41598-021-03217-8

Humbert M (1966) Carte géotechnique de Fès (1/20000): Royaume du Maroc, Ministère de l'industrie et des mines, Direction des mines et de la géologie, Division de la géologie, Service d'études des gîtes minéraux

Ishak M, Zolkepli M, Masyhur E et al (2022) Interrelationship between borehole lithology and electrical resistivity for geotechnical site investigation. Phys Chem Earth Parts a/b/c 128:103279. https://doi.org/10.1016/j.pce.2022.103279

Jeannette A (1965) Carte géotechnique de la meseta côtière à l'est de Casablanca (1/50000): Royaume du Maroc, Ministère de l'industrie et des mines, Direction des mines et de la géologie, Division de la géologie, Service d'études des gîtes minéraux

Karastathis VK, Karmis P, Novikova T et al (2010) The contribution of geophysical techniques to site characterisation and liquefaction risk assessment: Case study of Nafplion City, Greece. J Appl Geophys 72:194–211. https://doi.org/10.1016/j.jappgeo.2010.09.003

Khadrouf I, El Hammoumi O, El Goumi N, Oukassou M (2024) Contribution of HVSR, MASW, and geotechnical investigations in seismic microzonation for safe urban extension: A case study in Ghabt Admin (Agadir), western Morocco. J Afr Earth Sc 210:105138

Lin C-P, Lin C-H, Wu P-L et al (2015) Applications and challenges of near surface geophysics in geotechnical engineering. Chin J Geophys 58:2664–2680. https://doi.org/10.6038/cjg20150806

Loke MH, Barker RD (1996) Rapid least-squares inversion of apparent resistivity pseudosections by a quasi-Newton method[1]. Geophys Prospect 44:131–152. https://doi.org/10.1111/j.1365-2478.1996.tb00142.x

Loke MH (2004) Tutorial: 2-D and 3-D electrical imaging surveys, pp 29–31

Malki M, Choukr-Allah R, Bouchaou L, et al (2016) Assessment of groundwater quality: impact of natural and anthropogenic contamination in Souss-Massa River Basin, pp 1–20

Mazéas J-P (1967) Carte géotechnique de Safi (1/50000): Royaume du Maroc, Ministère de l'industrie et des mines, Direction des mines et de la géologie, Division de la géologie, Service d'études des gîtes minéraux

Mohammed MA, Abudeif AM, Abd El-Aal AK (2020) Engineering geotechnical evaluation of soil for foundation purposes using shallow seismic refraction and MASW in 15th Mayo, Egypt. J Afr Earth Sci 162:103721. https://doi.org/10.1016/j.jafrearsci.2019.103721

El Morjani ZEA, Ennasr M, Elmouden A et al (2016) Flood hazard mapping and modeling using GIS applied to the Souss River Watershed, pp 1–37

Mott PH, Dorgan JR, Roland CM (2008) The bulk modulus and Poisson's ratio of "incompressible" materials. J Sound Vib 312:572–575. https://doi.org/10.1016/j.jsv.2008.01.026

Muztaza NM, Ismail NA, Mohamad ET et al (2022) Seismic refraction assessment for excavatability and volume estimation in Kota Tinggi, Johor, Malaysia. J Appl Geophys 200:104612. https://doi.org/10.1016/j.jappgeo.2022.104612

Parry RHG (1977) Estimating bearing capacity in sand from SPT values. J Geotech Eng Div 103:1014–1019. https://doi.org/10.1061/AJGEB6.0000484

Pegah E, Liu H (2016) Application of near-surface seismic refraction tomography and multichannel analysis of surface waves for geotechnical site characterizations: a case study. Eng Geol 208:100–113. https://doi.org/10.1016/j.enggeo.2016.04.021

RPS (2011) Le reglement de construction parasismique. Ministère de l'ATUHE, Secrétariat d'État à l'Habitat, Rabat, Maroc Report RPS2000

Sébrier M, Siame L, Zouine EM et al (2006) Active tectonics in the Moroccan High Atlas. CR Geosci 338:65–79. https://doi.org/10.1016/j.crte.2005.12.001

Shang Y-J, Yang C-G, Jin W-J et al (2021) Application of integrated geophysical methods for site suitability of research infrastructures (RIs) in China. Appl Sci 11:8666. https://doi.org/10.3390/app11188666

Silva PG, Elez J, Pérez-López R et al (2021) The AD 1755 Lisbon Earthquake-Tsunami: seismic source modelling from the analysis of ESI-07 environmental data. Quat Int. https://doi.org/10.1016/j.quaint.2021.11.006

Tahayt A, Mourabit T, Rigo A et al (2008) Mouvements actuels des blocs tectoniques dans l'arc Bético-Rifain à partir des mesures GPS entre 1999 et 2005. Comptes Rendus Geoscience C R Geosci 340:400–413. https://doi.org/10.1016/j.crte.2008.02.003

Telford WM, Geldart LP, Sheriff RE, Keys DA (1976) Applied geophysics. Cambridge Univ. Press, New York, pp 1–860

Timoulali Y, El Hilali M, Hosny A et al (2022) Joint inversion of receiver functions and surface wave dispersion velocities to investigate the crustal structure of north of Morocco: case of Rif domain. Med Geosc Rev 4:537–554. https://doi.org/10.1007/s42990-022-00084-x

Toksoz MN, Cheng CH, Timur A (1976) Velocities of seismic waves in porous rocks. Geophysics 41:621–645

Uyanık O (2011) The porosity of saturated shallow sediments from seismic compressional and shear wave velocities. J Appl Geophys 73:16–24

Uyanık O (2019) Estimation of the porosity of clay soils using seismic P- and S-wave velocities. J Appl Geophys 170:103832. https://doi.org/10.1016/j.jappgeo.2019.103832

Watkins JS, Walters LA, Godson RH (1972) Dependence of in-situ compressional-wave velocity on porosity in unsaturated rocks. Geophysics 37:29–35. https://doi.org/10.1190/1.1440249

Zaid H, Arifin M, Mohd Nazer NS et al (2022) Geophysical investigation for engineering construction assessment in Karst area. Phys Chem Earth Parts a/b/c 129:103329. https://doi.org/10.1016/j.pce.2022.103329